

## *Chapter 1*

# Thesis Introduction

Sea level rise. Tipping points. Global warming. Today, the field of glaciology is irrevocably linked to the study of climate change, from the ivory tower to the network news. However, beyond attempts to quantify ice melting rates and predictions of the lifespans of dwindling glaciers, many aspects of the fundamental physics underlying the deformation of glaciers are poorly understood. Computational modeling of the response of glaciers in Greenland and Antarctica to hydrologic forcing over a timescale shorter than one month is the focus of this thesis. The results presented here are almost completely based on computational modeling but the goal is to explain several field observations of outlet glaciers and ice streams in the published literature. The interaction between ocean tides and ice stream motion (chapters 2, 3, and 4) and the rapid drainage of supraglacial meltwater lakes are the two glacial processes on which this thesis focuses.

The introductory section describes the Earth's cryosphere, focusing on the current scientific interest in glacier dynamics. The next section outlines the classical treatment of ice dynamics—both for general ice masses and the specific case of ice streams. The introduction then summarizes the current understanding of the interaction between the ocean tides and outlet glaciers, specifically over timescales shorter than a month. The next section discusses observations of the tidal influence on outlet glaciers from Antarctica and Greenland. The penultimate introductory section is a brief synopsis of the

finite element modeling methods used throughout this thesis. Last is a short outline of the remainder of this thesis.

## 1.1 The Cryosphere

The term *cryosphere* refers to all frozen water on planet Earth. While sea ice, river and lake ice, snow, and permafrost all belong to the cryosphere, glacial ice dominates the system. A *glacier* refers to any mass of crystalline ice that both persists over the course of an entire year and is large enough to flow under its own weight. The largest glaciers on the planet are the Antarctic and Greenland Ice Sheets, which together contain nearly 85% of all the freshwater on the planet (e.g., SMIC Report, 1971; L'vovich, 1979; IPCC, 1990; 1996; Van der Veen, 1999).

In the past few decades, the specter of global climate change has driven a renewed interest in the cryosphere, focusing on the fact that water in the cryosphere, primarily in the Greenland and Antarctic Ice Sheets, is equivalent to about 65 meters of sea level equivalent height (e.g., Cuffey and Paterson, 2010; Lythe et al., 2001; Bamber et al., 2001; Meier et al., 2007; Dyurgerov and Meier, 2005). As highlighted by the International Panel on Climate Change's (IPCC's) Fourth Assessment Report (2007), the lack of understanding of the interaction between the cryosphere and hydrosphere (i.e., ice sheets and the ocean) is a key piece of missing information that limits the believability of forward, predictive climate modeling. Upwards of 60% of the ice leaving the Greenland Ice Sheet and upwards of 90% of the ice leaving the Antarctic Ice Sheet is carried through a limited number of fast moving outlet glaciers, thus understanding the dynamics of these outlet glaciers is critical to predicting future ice levels (e.g., Cuffey and Paterson, 2010; Morgan et al., 1982; Bauer, 1961; Rignot and Kanagaratnam, 2006). The focus of

the first two research chapters is the interaction of these outlet glaciers and the short-term ocean tides.

We use Cuffey and Paterson (2010) as the reference for defining the characteristics of outlet glaciers. The technical definition of an *outlet glacier* is a fast-moving region of ice bounded by visible rock; an *ice stream* is a fast-moving region of ice bounded only by slower-moving ice. However following the convention of Cuffey and Paterson (2010), these terms are used interchangeably. The distinction between outlet glaciers and ice streams is generally too strict for practical use as many glaciers transition between ice-ice and ice-rock boundaries over their lengths. Note that while ice streams and outlet glaciers almost always flow into the ocean, the presence of a floating ice shelf or ice tongue is not a defining characteristic. Figure 1.1 shows the locations of all the ice streams discussed in this thesis.

As mentioned earlier, the majority of ice leaving the Greenland and Antarctic Ice Sheets travels through outlet glaciers. Direct calving of icebergs and basal melt are two of the primary mechanisms for removal of ice mass (e.g., Jacobs et al, 1992; Vaughan and Doake, 1996; Reeh et al., 1999; Mote, 2003; Wild et al., 2003; Hanna et al., 2005; Box et al., 2006; Krinner et al., 2006; Rignot et al., 2008; Cuffey and Paterson, 2010). Calving occurs when fractures propagate through the ice thickness at the edge of a glacier, resulting in blocks of ice shearing off the main ice body. Usually these new icebergs are carried out to sea, where they eventually melt. Basal melting occurs due to frictional heating along the base of grounded ice, melting due to geothermal heat along the base (e.g., subglacial volcanism, such as in Iceland), and the melting of floating ice shelves due to warmer ocean water reaching the ice's base.

Over long timescales, changes in the climate system can dramatically impact the response of ice streams to the conditions of the ocean. Increased melting, both on-land and at the grounding line due to higher ocean temperatures, reduces ice in the ice stream system and lubricates the ice stream's base, further increasing flow speeds. The combination of increased flow speeds and increased basal melt can thin ice streams to the point that any attached ice shelf breaks up. Ice shelf breakup in turn causes increased ice stream speeds due to the removal of the buttressing stress of the ice shelf, as was observed in the 1995 breakup of the Larsen A Ice Shelf and the 2002 breakup of the Larsen B Ice Shelf in Antarctica (Rott et al., 2002; De Angelis and Skvarca, 2003; Rignot et al., 2004, Scambos et al., 2004). Thus, the long-term behavior (and future) of ice shelves is linked to the interaction, and potential feedback, between the cryosphere and the earth's oceans.

However, the loss of ice through outlet glaciers is not the only mechanism for removing mass from the Greenland and Antarctic Ice Sheets on yearly timescales. Surface melt accounts for about 40% of the ice lost from Greenland and about 10% of the ice lost from Antarctica each year (e.g., Box et al., 2006; Krinner et al., 2006; Cuffey and Paterson, 2010). While this mass loss alone is significant, there is evidence from Greenland that supraglacial meltwater, should it reach the glacier's bed, can increase ice flow rates (e.g., Zwally et al., 2002; Joughin et al., 2008). The potential for such a feedback to cause a dramatic increase in the loss of ice mass with increasing temperatures (and thus melt rates) is not fully established, but modeling suggests that the effect can increase the mass-loss by upwards of a factor of two (Parizek and Alley, 2004).

Ultimately, while this thesis is not a direct study of the interaction of the cryosphere and the global climate system, that connection is the background motivation of this work. The hope is that the research presented here helps to elucidate some of the fundamentals of the response of ice to short timescale forcing. Understanding the hourly and daily dynamics of outlet glaciers requires more study. Through the investigation of tidal forcing of ice streams (chapters 2 to 4) and rapid drainage of supraglacial lakes (chapter 5), this thesis demonstrates some of the modeling concerns of processes that span the gap between very rapid (elastic) response on the order of days and more measured (viscous) response of ice streams on the order of years. The remainder of this introduction focuses on background information related to tidal forcing of ice streams, while the introductory material for the lake drainage problem is deferred to chapter 5 as that background material is unrelated to the remainder of this thesis.

## 1.2 Ice Stream Dynamics

This section provides a brief summary of ice stream dynamics. Information is presented from the introductory textbooks on glaciology by Van der Veen (1999) and Cuffey and Paterson (2010). A discussion of the general deformation of ice sheets and other non-streaming glaciers illustrates the unique nature of ice stream behavior. A description of the general physics in the extreme cases of ice stream geometry follows.

Consider a cross-sectional view of an ice sheet, as is shown in figure 1.2. The surface deformation at the location of a longitudinal cross section can be approximated by:

$$\vec{u} = \vec{u}_d + \vec{u}_b \quad (1.1)$$

where the total velocity vector  $\vec{u}$  is the additive sum of the internal deformation  $\vec{u}_d$  and the basal sliding  $\vec{u}_b$ .

In terms of internal deformation, we assume that glacier flow is driven by the weight of the ice itself, where the basal driving stress  $\tau_b$  for a vertical profile of the ice is:

$$\tau_b = \rho_i g H \sin(\alpha) \quad (1.2)$$

where  $\rho_i$  is the ice density,  $g$  is gravitational acceleration,  $H$  is the ice thickness, and  $\alpha$  is the surface slope. Assuming that ice deforms viscously over most timescales, that viscous deformation can be expressed using a canonical Glen-style flow law (Glen, 1955; 1958), and that glacier flow is laminar, we find that:

$$\vec{u}_d = \frac{2A_D}{n+1} (\tau_b)^n H \quad (1.3)$$

The value for the stress exponent  $n$  is traditionally chosen to be equal to three based on laboratory stress-strain curves (e.g., Glen, 1955; 1958).

To approximate basal sliding, we use the Weertman sliding law (Weertman, 1957; 1964), which assumes that the ice/bed interface is smooth and lubricated, save for a set of cubic bumps located at a regular interval. The resulting form of the sliding law, lumping many model parameters into the value  $A_W$ , is:

$$\vec{u}_b = A_W \tau_b^{\frac{n+1}{2}} \quad (1.4)$$

Such a sliding law is only applicable to glaciers that have a hard (i.e., rock) bed, as a soft, deformable till layer will behave differently. Observationally, most ice sheets are both slow moving and poorly lubricated at their bed, and thus are dominated by the internal deformation of the ice body (Cuffey and Paterson, 2010).

We are now equipped to comment on the dynamics of ice streams. Unlike ice sheets proper, ice streams are characterized by rapid velocities (e.g., Mae, 1979; Alley et

al., 1986; Bindschadler et al, 1986; Blankenship et al., 1986; Bindschadler et al, 1987; Shabtaie and Bentley 1987; 1988; Engelhardt et al., 1990; Engelhardt and Harrison, 1990; Alley and Whillans, 1991; Echelmeyer et al., 1991; Kamb, 1991; Echelmeyer et al., 1992; Iken et al., 1993; Funk et al., 1994; Clarke and Echelmeyer, 1996; Whillans and van der Veen, 1997; Sohn et al., 1998; van der Veen, 1999; Joughin et al, 2001; Kamb, 2001; Raymond et al., 2001; Lüthi et al., 2002; Thomas et al., 2003; Thomas, 2004; Joughin et al., 2004a/b; Cuffey and Paterson, 2010; many others). Apart from their rapid motions, ice streams can be quite diverse in character. On one end of the spectrum are the ice streams of the Siple Coast, Antarctica, or Rutford Ice Stream, which are characterized by very low surface slopes (and thus low driving stresses), heavily crevassed ice-ice lateral margins and a deformable till base. These ice streams are also extraordinarily long, reaching lengths of at least a few hundred kilometers in some cases. On the other end of the ice stream spectrum are the outlet glaciers found in Greenland, such as Helheim and Jakobshavn Isbrae. These ice streams are short, steep (high driving stress), and bounded by ice-rock margins along the confining fjords through which these outlet glaciers flow. Figure 1.3 shows satellite imagery of the Siple Coast, Rutford Ice Stream and Helheim Glacier. We discuss the dynamics of each separately as end-member possibilities.

The low driving stresses on the West Antarctica ice streams of the Siple Coast, as small as 20 kPa (Alley and Whillans, 1991), necessarily implies essentially zero basal tractions on these ice streams. From equations 1.3 and 1.4, we see this means very small amounts of internal deformation and very little sliding along the ice-bed interface (assuming a Weertman sliding law). Therefore, the observed rapid ice velocities must be

accounted for through deformation of the substrate beneath the ice streams. Numerous studies suggest that there is both a well-hydrated till layer beneath the Siple Coast ice streams, and that this till layer readily deforms plastically (e.g., Alley et al., 1986; Engelhardt et al., 1990; Kamb, 1991; Engelhardt and Kamb, 1998; Tulaczyk et al., 1998; 2000a/b; Kamb, 2001). In this configuration, the primary resistance to the ice stream's motion comes from the lateral margins of the ice streams, where the ice velocity rapidly falls by several orders of magnitude in the highly crevassed shear margins (Whillans et al., 1987; 1993; Whillans and van der Veen, 1993a/b).

Additionally, the ice streams of the Siple Coast are not flowing in a steady-state regime, as preserved paleo-glaciological features indicate different flow directions and orientations over the ice streams' existences (e.g., Conway et al., 2002; Retzlaff and Bentley, 1993; Clarke et al., 2000; Fahnestock et al., 2000; Gades et al., 2000; Joughin et al., 2004c). Furthermore, the velocity of ice streams can vary strongly over periods of centuries (Joughin et al., 2005). Cuffey and Paterson (2010) describes three hypotheses for the mechanism behind these long-timescale flow variations as: changes in ice stream geometry (e.g., Jacobson and Raymond, 1998), variations in basal water pressure (e.g., Raymond, 2000), and basal freeze-on resulting in stream stagnation (e.g., Alley et al., 1994; Tulaczyk et al., 2000b; Joughin et al., 2004b).

The fjord-constrained ice streams of Greenland are altogether different, primarily as the basal driving stress can reach values of 300–420 kPa due to the steep surface slopes (e.g., Clarke and Echelmeyer, 1996; Echelmeyer et al., 1991; 1992; Cuffey and Paterson, 2010). Estimates of Clarke and Echelmeyer (1996) suggest that frictional stress from the lateral margins balances between 10% and 50% of this driving stress, meaning

that the bed must support the remaining stress. Furthermore, these glaciers are assumed to lack the soft till beds that are found beneath Antarctic ice streams due to these large basal driving stresses, flowing instead along the hard rock bases of fjords. As there is no till layer to accommodate the driving stress, this stress partitioning necessary leads to internal deformation being more important to ice motion than basal sliding (compare equations 1.3 and 1.4 with a value of  $n=3$ ). This situation matches the modeling of Echelmeyer et al. (1991; 1992), which suggests that the internal deformation of Jakobshavn Isbrae is sufficiently large to explain the rapid ice velocity over most of the glacier, with basal sliding only necessary at the foot of the glacier where the driving stress drops due to shallower surface slopes. Thus, unlike the case of the Antarctic ice streams, the base of outlet glaciers in Greenland is thought to provide the primary resistance to flow.

### 1.3 Tidal Interaction with Grounded Ice

Section 1.1 described how the long-term variability in the interaction between outlet glaciers and ocean tides can impact the motion of the ice streams. Of course, the tides act on the solid earth in addition to the world's oceans. However, several factors argue against the importance of the *earth tides* in determining the tidal behavior of ice streams and outlet glaciers. First, the amplitude of the semidiurnal and diurnal earth tides are small at high and low latitudes, theoretically reaching a value of zero at the north and south poles for an idealized spherical earth. While such a simplification clearly does not hold for the real earth, studies of ocean and earth tides in Greenland and Antarctica suggest that the magnitude of the earth tide is at least an order of magnitude smaller than that of the ocean tides for these regions (e.g., Thiel et al., 1960; Zwally et al., 1983).

Second, the phase variation in the tidal response of many ice streams (as discussed below, e.g., Gudmundsson, 2006; 2007; de Juan, 2009; 2010a/b; de Juan Verger, 2011) suggests that the response is not caused by the earth tides, which acts roughly uniformly over the length-scales studied here (a few hundred kilometers). Thus, from this point forward, any reference to the tides will implicitly mean the ocean tides, unless otherwise specified.

Ocean tides obviously vary over timescales far shorter than those of sea level change, with the most relevant ocean tides being the semidiurnal, diurnal, and fortnightly tides. These short-period ocean tides directly control the motion of ice streams, foremost through the flexing of the ice stream due to the rising and falling of an attached ice shelf with the ocean tide. From surface observations, the spatial extent of ice flexure is limited to the first five to ten ice-thicknesses inland of the *grounding line*—the position where the ice stream transitions from floating to grounded ice (e.g., Rignot 1998a). Tidal flexure has been used primarily to constrain rheological parameters of *in situ* ice (assuming elasticity and, more recently, linear viscoelasticity). Such work derives values of Young modulus that are between three and ten times smaller from ice flexure than from laboratory experiments (e.g., Holdsworth, 1969; 1977; Lingle et al., 1981; Stephenson, 1984; Vaughan, 1994; 1995; Rignot 1996; 1998a/b; Reeh et al., 2000; 2003 compared against Petrenko and Whitworth, 1999). While useful for approximating rheological parameters, these flexure studies are essentially independent of the ocean tidal frequency, as these studies all focus on fitting the maximum tidal flexure amplitude and transmission.

A consequence of ice flexure during a tidal cycle is that the grounding line of an ice stream will necessarily move with the ocean tides, traveling further inland during high

tides and further seaward during low tides. As the exact amount of such a motion is dependent upon the slope and character of the ground beneath the ice stream, such behavior is inherently difficult to model. Observations from Antarctica (e.g., Rignot 1998a) suggest that the extent of this *grounding line zone* is approximately five kilometers—a distance equivalent to the flexural wavelength of an ice stream.

However, a more subtle interaction between the ocean tides and ice stream motion exists. Over the past two decades, glaciologists have accumulated a critical mass of tidally relevant observations such that the character of the tidal interaction with the flow of ice streams, especially at different frequencies, can now be broadly characterized. The next two subsections summarize such observational data, first from Antarctic ice streams and second from Greenland outlet glaciers.

### 1.3.1 Antarctic Tidal Interactions

Observations from Antarctica show tidally modulated surface displacements on some ice streams extend many tens of kilometers inland of the grounding line (see table 1.1 and associated references). Three classes of observations probe the interaction between ocean tides and the motion of ice streams: 1) surface tilt of the ice stream as estimated by tiltmeters, interferometric synthetic aperture radar (InSAR) and altimetric surveys; 2) surface recordings of basal seismicity beneath ice streams; 3) surface motion of ice streams from global position system (GPS) surveys. These observations can be used to identify which portion of an ice stream may be sensitive to tidal forcing (see table 1.1). Next is a summary of observations where the ocean tides do not have an impact on the motion of an ice stream far inland of the grounding line. While this thesis focuses on the observations of long distance transmission of tidal stresses, the usual tidal response of ice

streams is that the ocean tides only influence the motion of ice close to the grounding line.

### *Surface Tilt*

Surface tilt surveys quantify the maximum extent of tidal flexure of an ice body. The location of the change in curvature in ice surface due to the flexure of the ice stream is defined as the hinge line. The hinge line is found between five and ten kilometers inland for all ice streams in table 1.1 regardless of the specific method of determining hinge line location. For comparison, the hinge line is farther inland than the physical ungrounding of the ice stream due to increased flotation at high tide, which extends about five kilometers as an upper boundary for stable tidal modulation (e.g., Rignot, 1998a).

### *Seismicity*

Seismic studies on several Siple Coast ice streams correlate fluctuations in basal seismicity to the semidiurnal and/or fortnightly ocean tides. As these seismic triggers have been located at the base of the ice stream, there is probable cause to search for a link between the ocean tidal loading and the basal stress state in these ice streams. The rationale is as follows: ice slides frictionally over its bed, triggering seismicity due to asperities at the ice-bed interface. Changes in ocean tides can perturb the stress balance at the base of the ice stream by modifying the basal shear stress (e.g., Anandakrishnan et al., 1997; Bindschadler et al., 2003; Cuffey and Paterson, 2010). The rate of seismicity should correlate positively with the rate of motion, meaning that as basal shear stress increases, so too should the ice velocity, and thus the seismicity at the ice-bed interface.

The first suggestion of possible tidal variation in the observed seismicity beneath an ice stream came from Harrison et al. (1993). Harrison et al. suggests that ocean tides

may influence seismicity on Whillans Ice Stream at a single station 300 kilometers away from the nearest grounding line through the subglacial hydrologic network. This locale is somewhat anomalous in the observations of ocean tidal influence on ice streams due to its extreme distance inland of the grounding line. We are hesitant to use this site as a robust marker of tidal influence for three reasons. First, the authors note that the strain amplitudes are independent of the tidal amplitudes, a result unexpected for true tidal influence. Second, the authors also point out that the tidally variable strain appears and disappears seasonally whereas the ocean tides obviously do not. Third, the distance inland of this data point is in direct opposition to a limit set by the constraint provided by the geodetic survey of Winberry et al. (2009) described in section 2.2.3. As a result, we note the potential for tidal signal described in Harrison et al. (1993) for completeness, but we do not use it as an observational constraint for the purposes of ground-truthing our model results.

Observations from a three station seismic survey described in Anandkrishnan et al. (1997) limit the spatial extent of tidal sensitivity on Kamb Ice Stream to between 86 kilometers and 126 kilometers inland from the grounding line. The authors find that the frequency of subglacial seismic events correlates temporally with low tides within the nearby Ross Sea. Figure 1.4 shows an adaptation of figure 4 of Anandkrishnan et al. (1997) for the purpose of describing the observation. This figure shows the seismicity at a station 10 kilometers inland of the grounding line. While the seismicity peaks do not correspond one-to-one with the diurnal low tides, all the spikes in seismicity fall at these times. Of note is that the signal seems to be independent of the fortnightly variability in the tidal amplitude. Finally, the authors note that the Kamb Ice Stream is likely devoid of

subglacial water in the region of tidal modulated icequakes (based on Rose, 1979; Atre and Bentley, 1993; Anandakrishnan and Alley, 1994), implying that the connection between the ocean tides and the basal seismicity is carried through the bulk of the ice stream rather than through the subglacial hydrologic network.

Bindschadler et al. (2003) observed stick-slip generated seismicity on Whillans Ice Plain, a fact corroborated by the later studies of Wiens and other (2008) and Walter et al. (2011). These latter two studies disagree on the location of the nucleation of the observed stick-slip events, locating the seismicity either 10 or 50 kilometers inland of the grounding line of Whillans Ice Plain. In either case, stick-slip motion begins at an assumed asperity at the nucleation point and then propagates radially inland from there.

### *Geodesy*

Temporally continuous GPS (CGPS) surveys on some Antarctic ice streams find surface velocities modulating at a variety of tidal frequencies. Here, we review data from Rutford Ice Stream (Gudmundsson, 2006; 2007), Bindschadler Ice Stream (Anandakrishnan et al., 2003), and the Whillans Ice Plain/Ice Stream (Wiens et al., 2008; Winberry et al., 2009). For Rutford and Bindschadler Ice Streams, the tidal influence manifests itself as a variable tidal displacement in the flow direction when the GPS signal is de-trended for the linear motion of the ice towards the grounding line. On the Whillans Ice Plain and Ice Stream, the ocean tides modulate the timing of the onset of stick-slip motion, roughly in phase with the maxima and minima of the tides.

As the CGPS surveys are the most temporally-refined method of observing the tidally-induced motion of these ice streams, we focus on these data as our primary constraints. As the ice streams are rapidly flowing, the GPS signal has a strong linear

trend associated with the background flow velocity, which over the timescales studied here is roughly constant. By subtracting the background flow rate (i.e., the displacement due to the average ice flow), any remaining displacement signal must be due to other processes, the foremost of which is the influence of ocean tides. Figure 1.5 shows such a process for a few selected GPS stations from the Whillans Ice Stream as a representative case (data provided by S. Anandakrishnan and H. Gudmundsson).

All the studies discussed here involve GPS surveys with stations either placed linearly along the flow line of the ice stream (Rutford, Bindschadler, and Whillans Ice Streams) or in a grid across the ice stream (Whillans Ice Plain). Thus, the relative amplitude of displacement due to the tidal load as a function of distance is fairly well constrained. All the surface displacements corresponding to the tidal modulated motion decay with distance inland from the grounding line with decay length-scales (for an order of magnitude drop) on the range of 35 to 75 kilometers, as shown in figure 1.6 (data from Anandakrishnan et al., 2003; Gudmundsson, 2006; 2007). For the ice streams in question, the maximum inland distances where a discernible tidal signal in the surface displacement is seen are: 40 kilometers inland of the grounding line for Rutford Ice Stream, 80 kilometers inland of the grounding line for Bindschadler Ice Stream, and from the spatial distribution of tidal-frequency stick-slip events, at least 100 kilometers inland of the nearest grounding line for the Whillans Ice Plain.

An additional major constraint on the tidally-induced surface motion of these ice streams is the phase lag between the observed tidal displacement signal and the peak tidal amplitude. As part of the aforementioned studies, at least one GPS station was placed on floating ice. In each study, the vertical displacement of this floating station functionally

became the tidal record. When the GPS records at the inland sites are de-trended to remove the background flow, we can measure an apparent phase-shift between the tidal frequencies seen in the floating tidal signal and the grounded surface displacement records.

For Rutford Ice Stream, Gudmundsson (2006; 2007) demonstrates that there is a distance dependent phase lag in the signal, such that the phase of all tides (semidiurnal, diurnal, and fortnightly) increases with inland distance. For reference, these studies define a zero-phase ice response as having the peak outboard de-trended ice motion contemporaneous with the high tide from the tide model T\_Tides (Pawlowicz et al., 2002). Additionally, the phase is between 45 and 270 degrees behind the tidal signal, suggesting that the high tide corresponds roughly with the maximum (de-trended) inland displacement in the GPS records. Additionally, a non-zero phase is seen even on the floating ice shelf, meaning that the motion of the glacier is never in-phase with the ocean tides. From GPS data on Bindschadler Ice Stream, Anandakrishnan et al. (2003) found that the relative phase lag in the ice response to the diurnal tide grows from  $1.1 \pm 2$  hrs ( $16.5 \pm 30$  degrees) at 40 kilometers inland to  $3.1 \pm 2$  hrs ( $46.5 \pm 30$  degrees) at 80 kilometers inland, similarly showing a distance dependence to the phase lag. For the Whillans Ice Stream and Plane, the stick-slip motion of the ice makes determining a phase lag in the displacement signal untenable.

#### *Contrary Observations*

Not all Antarctic ice streams show measurable tidal modulation of surface displacements upstream of their hinge lines. CGPS observations on Pine Island Glacier, for example, show no tidal variability in surface motion at stations 55, 111, 169, and 171 kilometers

inland of the grounding line (Scott et al., 2009). Ekstrom Ice Shelf has an even tighter constraint on the spatial extent of tidal perturbations: CGPS recordings only one kilometer inland of the grounding line possess no measurable component of motion at tidal frequencies (Riedel et al., 1999; Heinert and Riedel, 2007). As will be discussed in the next section the spatially-limited transmission of a tidal signal on these Antarctic ice streams is similar to outlet glaciers in Greenland.

### 1.3.2 Greenland Tidal Interactions

Direct observations of short-timescale tidal influence on the behavior of outlet glaciers in Greenland are more limited than those from Antarctica. GPS studies investigating the floating portion of Kangerdlugssuaq and Helheim Glaciers reveal flow velocities that fluctuate with ocean tides (Hamilton et al., 2006; Davis et al., 2007; de Juan et al., 2009; 2010a/b; de Juan Verger, 2011). Of this work, the largest single GPS survey is the geodetic survey of Helheim Glacier from 2006–2009, comprised of 23 GPS stations arrayed over the length of Helheim Glacier (de Juan, 2009; 2010a/b; de Juan Verger, 2011).

From the aforementioned geodetic survey, de Juan Verger (2011) was able to characterize the tidal interaction of Helheim glacier based on the admittance amplitude (relative magnitude of tidally-induced glacier displacement to the ocean tidal amplitude) and the phase lag between the GPS receivers on the lower portion of Helheim glacier and a tidal record from within the Sermilik Fjord (into which Helheim Glacier flows). The admittance amplitude decays exponentially with distance inland from the glacier's calving front with a phase lag of 0–4 hours (0–120 degrees). For the purposes of this summary, we divide the survey into two portions: first, the 2006 records, where Helheim

Glacier had a floating ice tongue; and second, the 2007-2008 survey, where Helheim Glacier has no floating ice tongue.

During the 2006 survey when Helheim Glacier had a floating ice tongue, de Juan Verger (2011) reports that there is a tidal signal in the along-glacier, cross-glacier, and vertical directions. In all cases, the signal decays exponentially with distance away from the glacier's edge, with the cross-glacier and vertical components decaying over an e-folding length of about 1.0 kilometers, while the along-glacier length-scale is about 2.3 kilometers. These distances translate to an order of magnitude drop in stress over a length of 3.7 kilometers and 8.5 kilometers, respectively. For reference, the thickness of Helheim Glacier was approximately 750 meters during these surveys (de Juan Verger, 2011). The de-trended response of Helheim Glacier to the semidiurnal ocean tides is out of phase, such that at high tide the de-trended position of Helheim Glacier is farther inland than at low tide. However, there is additional lag between this response and the semidiurnal ocean tides, such that the peak glacier motion is delayed relative to the peak tidal amplitudes. The best fit phase lag between the response of the along-glacier displacement and the tide gauge ranges between about 1 hour and 2 hours (30-60 degrees), though a large error on some data points allows for a range that may extend between 0 and 4 hours (0-120 degrees). The best fit values suggest an increase in phase lag with distance inland, but such a trend is dubious at best as the magnitude of the distance-variation falls below the errors of the fits.

For the grounded glacier surveys during 2007-2008, de Juan Verger (2011) reports that there is essentially no tidal signal in the cross-glacier and vertical directions, while the e-folding length-scale for the along-glacier admittance amplitude is around 4.2

kilometers for the two years. This decay rate translates to an order of magnitude drop in amplitude over a distance of around 15.3 kilometers. As in the 2006 survey, the response of Helheim Glacier is out of phase with the semidiurnal ocean tide, with the best fit phase lags falling between 2 and 3 hours (60–90 degrees) with errors ranging from 0 to 4 hours (0–120 degrees). Similarly between surveys, there is a slight trend for increasing phase with the best fit phase values, but that this trend is well within the error of the observations. However, the mean values of the best fit do seem to indicate that the grounded ice may have an increased phase lag compared to the floating ice.

Apart from this work, the only other major observations of tidal forcing of Greenland outlet glaciers come from Jakobshavn Isbrae. On Jakobshavn Isbrae, the lowest reaches of the ice stream are found to have a variable velocity at tidal frequencies (up to 35%, Echemeyer and Harrison, 1990; 1991), but that the tidal amplitude of this signal decays rapidly inland of the ice stream terminus, with a characteristic length-scale of a few ice-thicknesses (Podrasky et al., 2002; 2012). Inland of this tidal signal there are variations in ice stream velocity, but Podrasky et al. (2012) accounts for these variations through seasonal melt rather than ocean tidal loading. There is no discussion of the relative phase of the glacial motion compared to the ocean tidal signal for Jakobshavn Isbrae within these works.

### 1.3.3 Observation Summary

To close our discussion of the observations of tidal influence on ice stream motion, we summarize the salient features of these tidal observations as:

- 1) Not all ice streams exhibit tidally modulated surface motion far from the grounding line. For example, Helheim Glacier has a tidal signal that is essentially

unseen beyond 14 kilometers inland of the calving front. However, some Antarctic ice streams transmit tidal signals many 10's of kilometers inland of the grounding line.

- 2) Tidal influence on ice motion happens over multiple timescales, often at semidiurnal, diurnal, and fortnightly periods. The ice stream seems to filter some of the tidal frequencies such that the de-trended GPS records do not exhibit many of the beat frequencies seen from the vertical component of GPS stations on floating ice.
- 3) The time-domain phase of the ice stream response can vary with distance inland of the ice stream's grounding line. Such temporal lag likely provides information about the rheology of the material transmitting the tidal stress inland. Furthermore, the phase lag is different over the various tidal frequencies.
- 4) Indirect measurement of ice stream motion, such as seismicity located at the ice stream's bed, indicate that basal processes are important to determining the motion of a given ice stream. However, the variability in seismicity on tidal periods implies that there is some connection between the tidal forcing on the ice stream and the frictional processes at the bed-ice interface.

## 1.4 General Finite Element Methods

Because we use finite element modeling throughout this thesis, we now depart from glaciology briefly to present a summary of the computational finite element methods here. In the later chapters, we will discuss project-specific modeling finite element formulation and model configurations. All of our finite element methods use the finite element analysis software *PyLith* (Williams et al., 2005; Williams, 2006; Aagaard et al.,

2007; 2008; 2011). This open-source Lagrangian FEM code has been developed and extensively benchmarked in the crustal deformation community (available at [www.geodynamics.org/pylith](http://www.geodynamics.org/pylith)).

*PyLith* solves the conservation of momentum equations with an associated rheological model. As we assume a quasi-static formulation (i.e., all inertial terms are dropped), the governing equations are:

$$\begin{aligned}\sigma_{ij,j} &= f_i \text{ in } V \\ \sigma_{ij}n_j &= T_i \text{ on } S_T \\ u_i &= u_i^0 \text{ on } S_U\end{aligned}\tag{1.5}$$

where  $V$  is an arbitrary body with boundary condition surfaces  $S_T$  and  $S_U$ . On  $S_T$ , the traction  $\sigma_{ij}n_j$  equals the applied Neumann boundary condition  $T_i$ . On  $S_U$ , the displacement  $u_i$  is set equal to the applied Dirichlet boundary condition  $u_j^0$ .

*PyLith* solves these equations using a Galerkin formulation of the spatial equation and an unconditionally stable method of implicit timestepping (following the form of Bathe, 1995). For model convergence, we select convergence tolerances in absolute and relative residual of the iterative solver from the *PETSc* library (Balay et. al, 1997; 2012a/b) such that our model results are independent of the convergence tolerances to a factor of less than 1/1000%. Such convergence tolerances are determined through trial-and-error with our model accuracy criterion chosen to provide reliable results while minimizing the computational time of any given model.

We construct our FEM meshes using the software *Cubit* ([cubit.sandia.gov](http://cubit.sandia.gov)). For our two-dimensional models, we use linear isoparametric triangular elements, while in our three-dimensional modeling we use linear isoparametric

quadrilateral or tetrahedral elements. We manually refine our meshes near regions of applied stresses, changes in boundary conditions, and material property variations. In such locations our mesh spacing can be as small as 1 meter, resulting in meshes with between  $10^5$  and  $10^6$  elements. To ensure that our results are independent of our meshing scheme, we check all our results against meshes that are uniformly refined. We only present results from meshes that have less than a 0.1% change in displacement, 1<sup>st</sup> strain invariant, and 2<sup>nd</sup> deviatoric stress invariant upon this refinement in our elastic models and less than 1% in our viscoelastic models. We allow a greater error in our viscoelastic modeling as the computational time necessary for a 0.1% error is restrictively long.

Our final modeling constraint is our choice of material rheology. We begin with a linear, isotropic elastic model for ice in our models that takes the familiar form of Hooke's Law in three dimensions:

$$\mathbf{C}_{ijkl} = \lambda \delta_{ij} \delta_{kl} + \mu (\delta_{ik} \delta_{jl} + \delta_{il} \delta_{jk}) \quad (1.6)$$

The choice of material moduli varies between our models; however, for all our models we assume that the Poisson's ratio is well known for ice (and thus is fixed) when exploring the ranges in values of the other elastic moduli. We also consider a Glen-style Maxwell viscoelastic rheology:

$$\dot{\epsilon} = \frac{\dot{\sigma}}{E} + A \sigma^n \quad (1.7)$$

As we vary the value of the viscosity coefficient  $A$  and the power law exponent  $n$  in our modeling, the selection of the precise values of these quantities will be discussed in each chapter separately.

## 1.5 Thesis Outline

This thesis is divided into four sections summarizing the results from three separate research projects undertaken between 2009 and 2013. In chapter 2, we test the common assumption that tidal loads are transmitted elastically through the bulk of ice streams to the long inland distances observed in Antarctica. We find that the geometric constraints of the ice stream itself limit the transmission of a tidal stress to distances far shorter than seen observationally. In chapter 3, we then explore the potential effect that including strain-weakened lateral margins and viscoelasticity in models has on the transmission length-scale.

Chapter 4 outlines a procedure for using geometrically simple finite element models and surface observations of tidally modulated glacier motion to constrain viscoelastic rheological parameters. We also explore the type, quantity, and quality of surface observations needed to provide an accurate constraint on the *in situ* material properties for outlet glaciers. We then provide a test example using GPS data from Helheim Glacier, Greenland.

Chapter 5 discusses our results from investigating the impact of viscoelastic deformation during transient drainage events of supraglacial lakes. We present both semi-analytic linear viscoelastic and finite element nonlinear viscoelastic modeling, using as a constraint observations from a 2006 lake drainage event near Jakobshavn Isbrae, Greenland.

At the end of each chapter, we include a list of all variables specific to that chapter. While many variables are shared between chapters, some variables have multiple definitions between chapters. Following the variable list are the figures and

---

tables discussed in the main chapter. The final portion of each chapter includes any associated appendices. For appendices with figures and tables, these are presented at the end of that appendix. Lastly, as many of the references are common between chapters, all references for the entire thesis are included at the end of the full document.

	Variable Names	Units
	$A$ Nonlinear viscosity coefficient	$\text{Pa}^{-n} \text{s}^{-1}$
	$A_D$ Ice deformation coefficient	$\text{Pa}^{-n}$
	$A_W$ Basal sliding coefficient	$\text{Pa}^{-(n+1)/2} \text{m}$
	$\mathbf{C}_{ijkl}$ Elasticity tensor	$\text{Pa}$
	$E$ Young's modulus	$\text{Pa}$
	$f_i$ Force vector	$\text{N}$
	$g$ Gravitational acceleration	$\text{m s}^{-2}$
	$H$ Ice sheet thickness	$\text{km}$
	$n$ Power law exponent	--
	$n_i$ Normal vector	--
	$S_T$ Traction boundary surface	--
	$S_U$ Displacement boundary surface	--
	$T_i$ Applied traction	$\text{Pa}$
	$\vec{u}$ Velocity vector	$\text{m/s}$
	$\vec{u}_b$ Basal sliding vector	$\text{m}$
	$\vec{u}_d$ Internal deformation vector	$\text{m}$
	$u_i$ Displacement component	$\text{m}$
	$u_i^0$ Applied displacement	$\text{m}$
	$V$ Model volume	$\text{m}^3$
	$\alpha$ Surface slope	$^\circ$
	$\delta_{ij}$ Kronecker delta	--
	$\varepsilon$ Strain	--
	$\lambda$ 1 <sup>st</sup> Lamé constant	$\text{Pa}$
	$\mu$ 2 <sup>nd</sup> Lamé constant	$\text{Pa}$
	$\rho$ Ice density	$\text{kg m}^{-3}$
	$\sigma$ Stress	$\text{Pa}$
	$\tau_b$ Basal stress	$\text{Pa}$

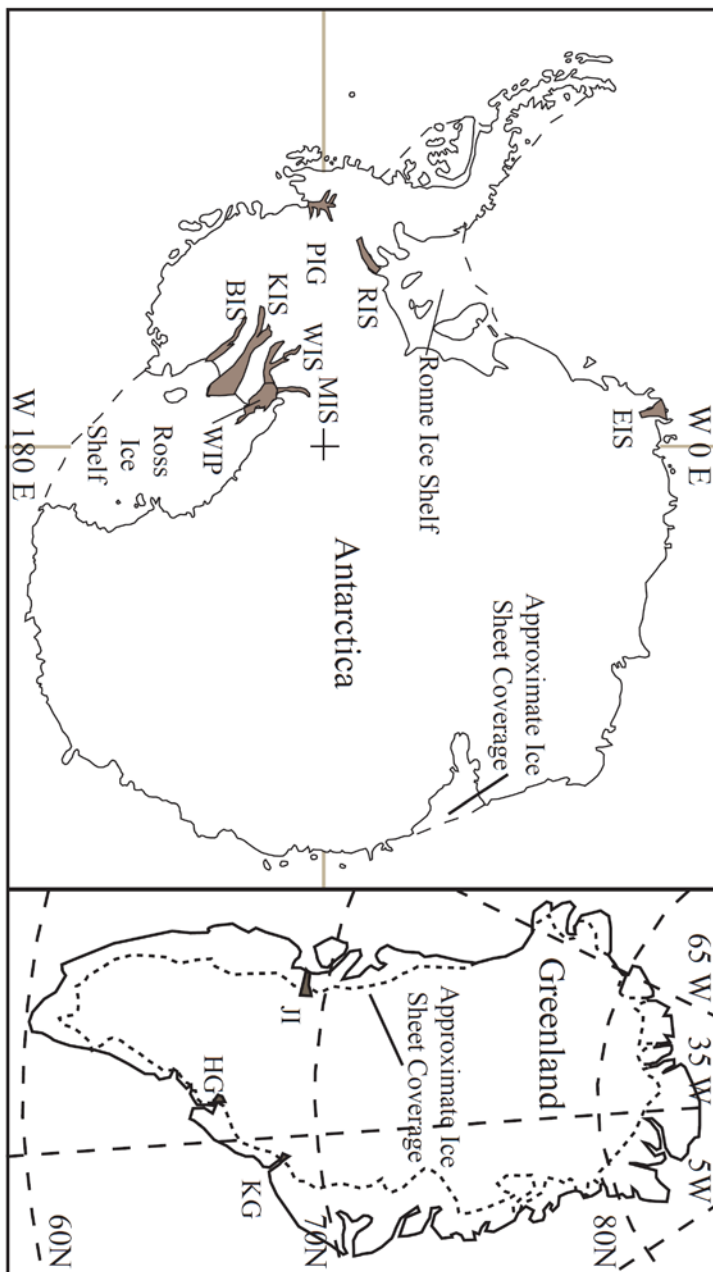


*Figure 1.1:* Location map of the ice streams discussed in this thesis. Abbreviations are EIS: Ekstrom Ice Shelf; RIS: Rutford Ice Stream; PIG: Pine Island Glacier; MIS: Mercer Ice Stream; WIS: Whillans Ice Stream; WIP: Whillans Ice Plain; KIS: Kamb Ice Stream; BIS: Bindschadler Ice Stream; JI: Jakobshavn Isbrae; HG: Helheim Glacier KG: Kangerdlugssuaq Glacier. Dashed outlines show the extent of glacial ice in both figures.

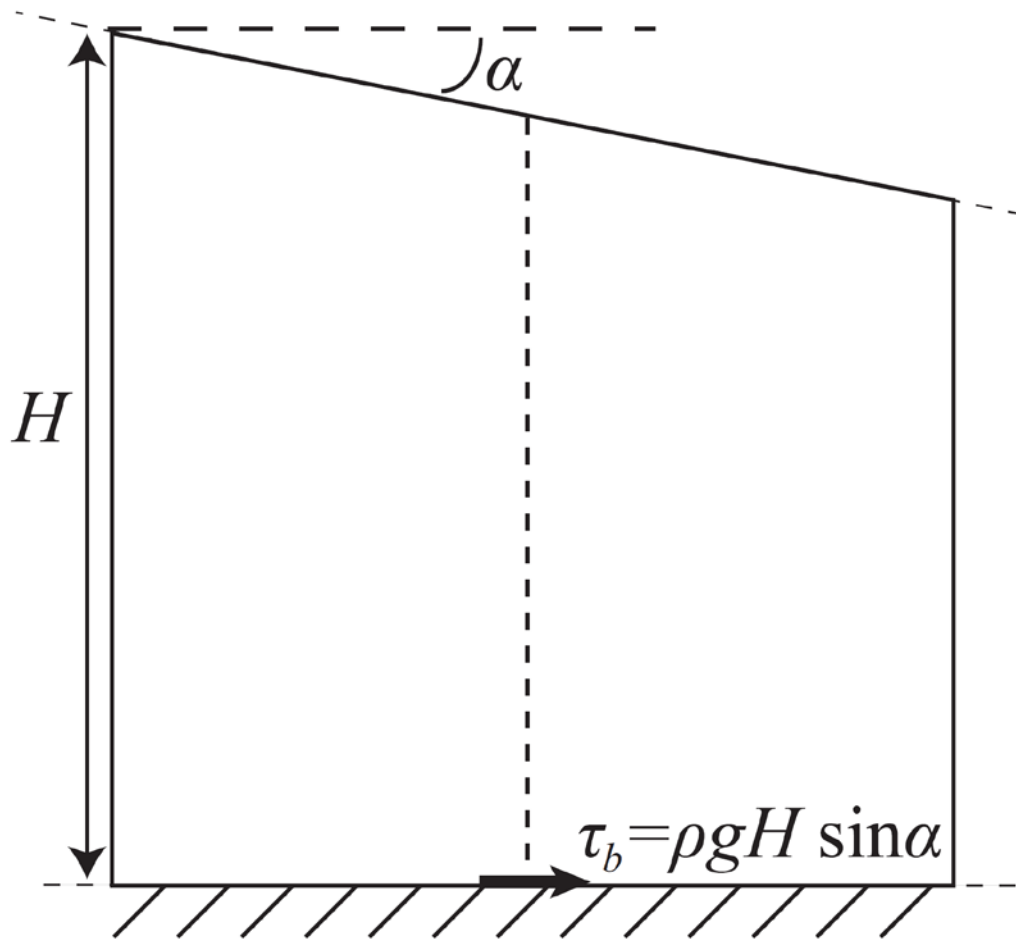


*Figure 1.2:* Schematic cross section of a simple ice sheet. The surface slope is denoted by  $\alpha$ , the ice thickness by  $H$ , and the basal driving stress by  $\tau_b$ . Note that the surface slope is greatly exaggerated in this figure for emphasis. The flow direction of the ice sheet is towards the right.

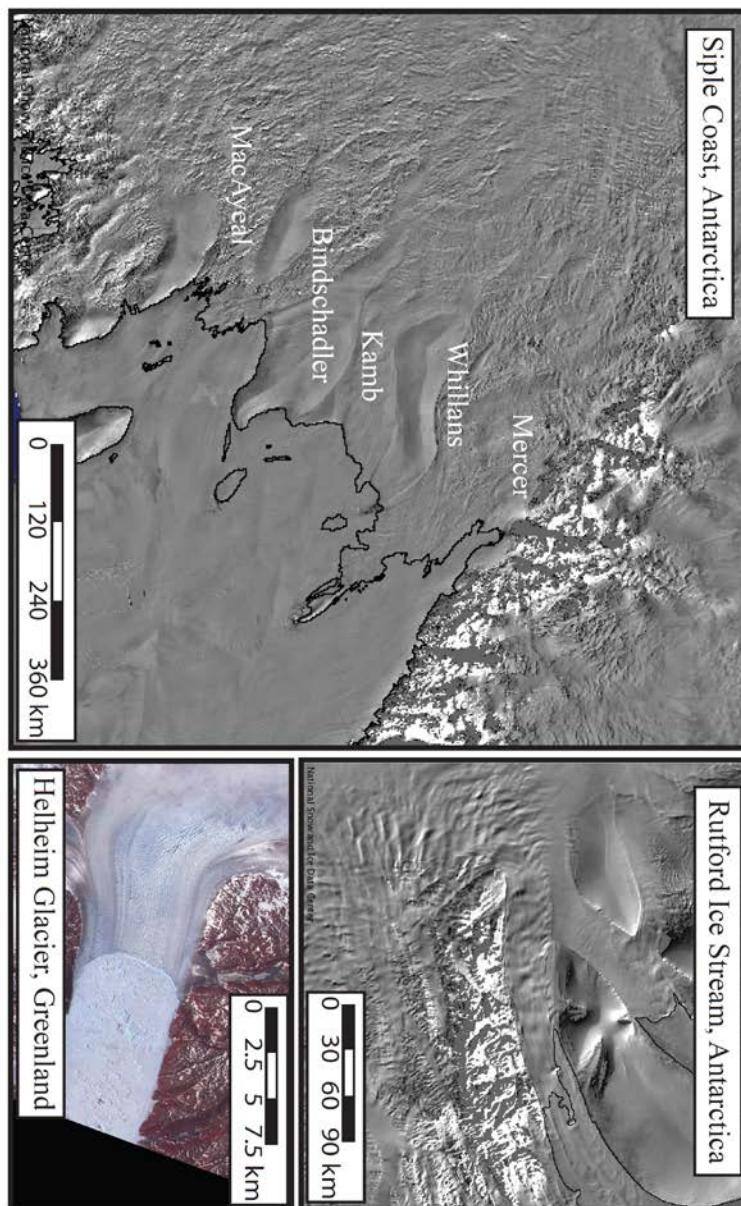


*Figure 1.3:* Satellite imagery of the specific ice streams discussed in this thesis. Note that the location of each panel is shown in figure 1.1. Imagery from the Siple Coast and Rutford Ice Stream are taken from the Atlas of the Cryosphere, a service provided by the National Snow and Ice Data Center (NSIDC). The satellite image for Helheim Glacier is from the January 20th, 2006 “Picture of the Day” from the NASA Earth Observatory website. The image uses data from Howat et al., 2005.

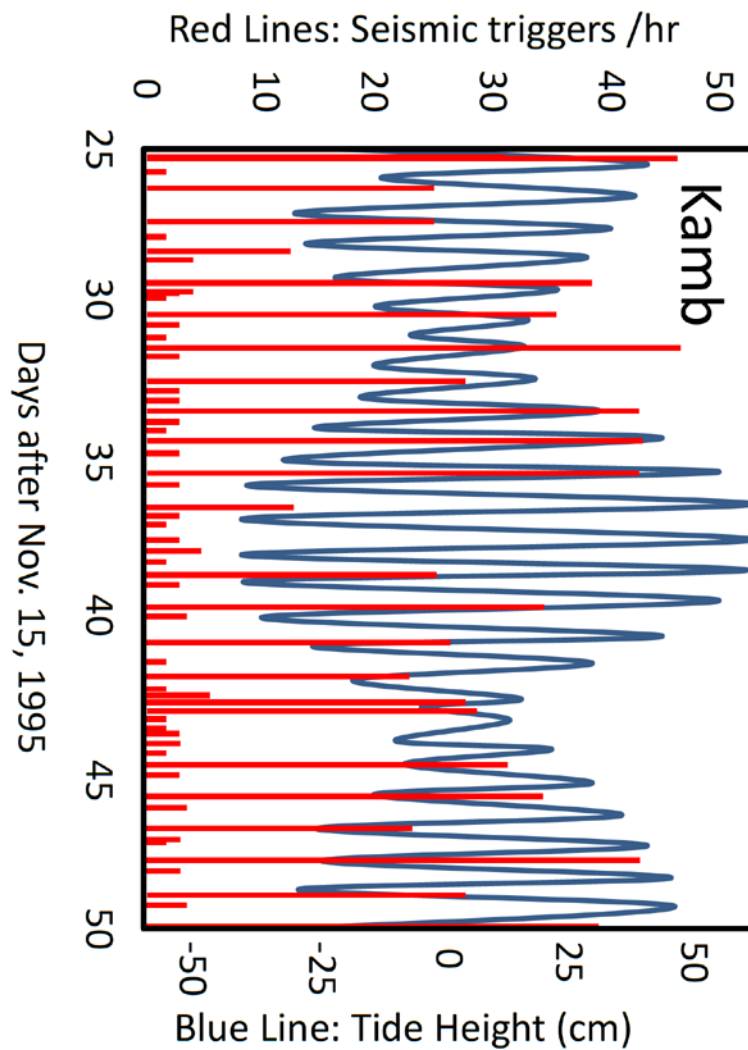


*Figure 1.4:* Seismicity on the Kamb Ice Stream, adapted from Anandakrishnan et al. (1997). The blue curve in the background shows the tidal signal from a tide meter, with the amplitude shown on the right side of the plot. The red lines show the seismicity rate as a number of triggered events per hour. Note that the peaks in seismic activity correspond to the peak tidal amplitudes.

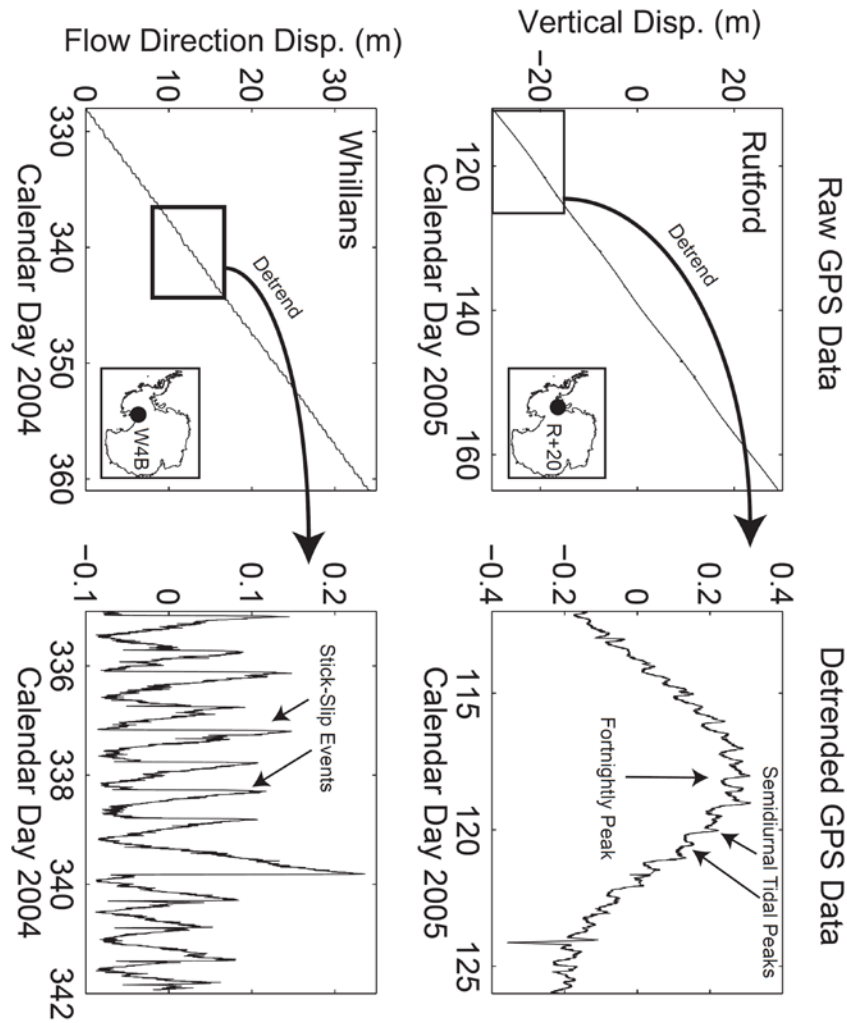
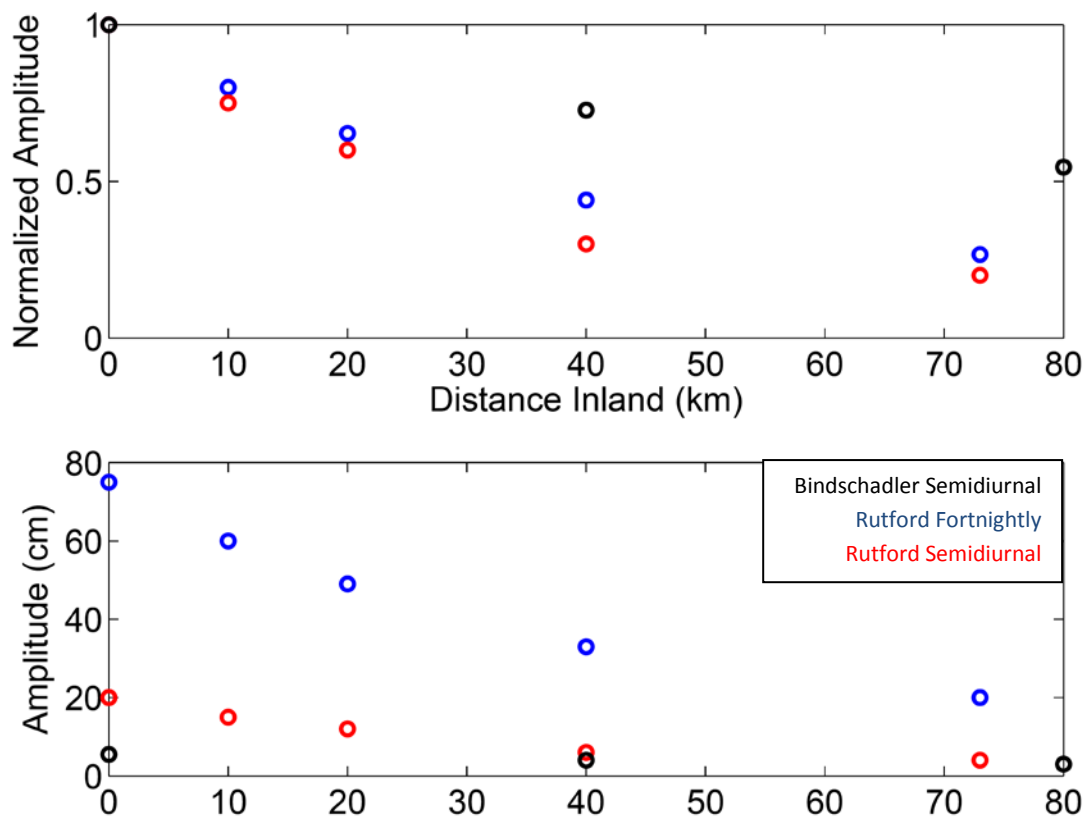


Figure 1.5: Sample GPS records from station R+20 from Rutford Ice Stream (upper figures) and W4B from Whillans Ice Plain (lower figures) for surface displacement rotated into the primary flow direction. The panels on the left show the raw GPS signal; note the strong linear trend in the GPS signal. The GPS records with this linear trend removed are shown in the figures on the right. For the Rutford Ice Stream, the tidal signal is shown as a sinusoidal variation in ice position. For the Whillans Ice Plain, the tidal variability triggers stick-slip events in the displacement record. Data is from H. Gudmundsson (Rutford) and S. Anandakrishnan (Whillans).



*Figure 1.6:* Amplitude of the tidal signal present in GPS stations on Rutford and Bindschadler Ice Streams as a function of distance inland from the grounding line. The upper panel shows the normalized amplitudes of the signal, while the lower panel shows the true amplitudes of the three datasets. The colors corresponds to: black-Bindschadler semidiurnal tidal amplitude, blue-Rutford fortnightly tidal amplitude, red-Rutford semidiurnal tidal amplitude.

<i>Ice Stream</i>	<i>Tidal Stress Transmission</i>		<i>Ice Flexure</i>	
	<i>Extent</i> ( <i>km</i> )	<i>Method</i>	<i>Extent</i> ( <i>km</i> )	<i>Method</i>
Bindschadler Ice Stream	80 +	GPS displacement <sup>1</sup>	~ 10	ICESat altimetry <sup>2</sup>
Ekstrom Ice Shelf	< 3	GPS displacement <sup>3</sup>	~ 5	Tilt <sup>3</sup>
Kamb Ice Stream	85 +	Seismicity <sup>4</sup>	~ 10	ICESat altimetry <sup>2</sup>
Pine Island Glacier	< 55	GPS displacement <sup>5</sup>	~ 5	SAR <sup>6</sup>
Rutford Ice Stream	40 +	GPS disp. <sup>7,8</sup>	5 +	Tilt <sup>9</sup>
Whillans Ice Plain	~ 100	GPS (stick-slip) <sup>10,11</sup> Seismicity <sup>10,12</sup>	~ 10	ICESat altimetry <sup>2</sup>
Whillans Ice Stream	~ 300	Seismicity <sup>13</sup>	N/A	ICESat altimetry <sup>2</sup>
Kangerdlussuaq	?	N/A	Var.	N/A
Helheim	< 10	GPS disp. <sup>14,15,16,17</sup>	Var.	N/A
Jakobshavn Isbrae	< 10	GPS disp. <sup>18,19</sup>	Var.	N/A

*Table 1.1:* Summary of the spatial extent of tidal stress transmission and ice flexure from ice streams across Antarctica and Greenland. Superscript numbers denote the following references: 1-Anandakrishnan et al. (2003); 2-Brunt et al. (2010); 3-Heinert and Riedel (2007); 4-Anandakrishnan and Alley (1997); 5-Scott et al. (2009); 6-Rignot (1998); 7-Gudmundsson (2006); 8-Gudmundsson (2007); 9-Stephenson (1984); 10-Weins et al. (2008); 11-Winberry et al. (2009); 12-Walter et al. (2011); 13-Harrison et al. (1993); 14-de Juan (2009); 15-de Juan (2010a); 16-de Juan (2010b); 17-de Juan Verger (2011); 18-Podrasky (2002); 19-Podrasky (2012). The flexure of the Greenland outlet glaciers is listed as variable as the flexure depends strongly on the size of the floating ice shelf, which for these glaciers has changed dramatically over the past decade.